RAB27A promotes melanoma cell invasion and metastasis via regulation of pro-invasive exosomes

Dajiang Guo[1,2]*, Goldie Y. L. Lui[1,2]*, Siew Li Lai[1], James S. Wilmott[2,3], Shweta Tikoo[1,2], Louise A. Jackett[2,3,4], Camelia Quek[3], Darren L. Brown[5], Danae M. Sharp[1,2], Rain Y.Q. Kwan[1,2], Diego Chacon[6,7], Jason H. Wong[7,8], Dominik Beck[6,7], Michelle van Geldermalsen[1,2], Jeff Holst[1,2], John F. Thompson[2,3,4], Graham J. Mann[3,9], Richard A. Scolyer[2,3,4], Jennifer L. Stow[5], Wolfgang Weninger[1,10,11#], Nikolas K. Haass[1,10,12#], Kimberley A. Beaumont[1,2#]

[1]The Centenary Institute, The University of Sydney, Newtown, NSW, Australia; [2]Sydney Medical School, The University of Sydney, Camperdown, NSW, Australia; [3]Melanoma Institute Australia, The University of Sydney, North Sydney, NSW, Australia; [4]Royal Prince Alfred Hospital, Camperdown, NSW, Australia; [5]The Institute for Molecular Bioscience, The University of Queensland, Brisbane, QLD, Australia; [6]Centre for Health Technologies and the School of Biomedical Engineering, University of Technology, Sydney, NSW, Australia; [7]Adult Cancer Program, Lowy Cancer Research Centre, Prince of Wales Clinical School, University of New South Wales, Sydney, NSW, Australia; [8]School of Biomedical Sciences, Li Ka Shing Faculty of Medicine, The University of Hong Kong, Pok Fu Lam, Hong Kong; [9]Centre for Cancer Research, Westmead Institute for Medical Research, The University of Sydney, Westmead, NSW, Australia; [10]Discipline of Dermatology, The University of Sydney, Camperdown, NSW, Australia; [11]Department of Dermatology, Royal Prince Alfred Hospital, Camperdown, NSW, Australia; [12]The University of

This article has been accepted for publication and undergone full peer review but has not been through the copyediting, typesetting, pagination and proofreading process, which may lead to differences between this version and the Version of Record. Please cite this article as doi: 10.1002/ijc.32064

Queensland, The University of Queensland Diamantina Institute, Translational Research Institute, Brisbane, QLD, Australia;

*these authors contributed equally to this work

#these authors contributed equally to this work

Correspondence:

Nikolas K. Haass, The University of Queensland Diamantina Institute, Translational Research Institute, 37 Kent St, Woolloongabba, QLD 4102, Australia. Phone +61 7 3443 7087; fax +61 7 3443 6966; e-mail: n.haass1@uq.edu.au

Kimberley A. Beaumont, The University of Queensland, St Lucia, QLD, 4072, Australia. Phone +61 7 3346 2378; e-mail k.beaumont@uq.edu.au

Short title: RAB27A promotes melanoma cell invasion and metastasis via exosomes.

Key words: exosomes, invasion, metastasis, melanoma, RAB27A

Abbreviations: DE: differential expression; EM: electron microscopy; FDR: false-discovery rate; FUCCI: fluorescence ubiquitination cell cycle indicator; GO: gene ontology; IHC: immunohistochemistry; IPA: Ingenuity Pathway Analysis; KEGG: Kyoto Encyclopedia of Genes and Genomes; KD: knockdown; KO: knockout; MIA: Melanoma Institute Australia; MVB: multivesicular body; TCGA: The Cancer Genome Atlas.

Article Category: Molecular cancer biology

Novelty and Impact (75 words):

Melanoma is the deadliest type of skin cancer, and metastasis is the primary cause of death. We show that high RAB27A expression correlates with poor patient survival. Importantly, we identify RAB27A as a driver of melanoma metastasis *via* the secretion of pro-invasive exosomes. We provide insight into the RAB27A-mediated regulation of cancer-promoting exosomes and propose RAB27A as a novel prognostic factor and therapeutic target for prevention of melanoma metastasis.

Abstract:

Despite recent advances in targeted and immune-based therapies, advanced stage melanoma remains a clinical challenge with a poor prognosis. Understanding the genes and cellular processes that drive progression and metastasis is critical for identifying new therapeutic strategies. Here, we found that the GTPase RAB27A was overexpressed in a subset of melanomas, which correlated with poor patient survival. Loss of RAB27A expression in melanoma cell lines inhibited 3D spheroid invasion and cell motility *in vitro*, and spontaneous metastasis *in vivo*. The reduced invasion phenotype was rescued by RAB27A-replete exosomes, but not RAB27A-knockdown exosomes, indicating that RAB27A is responsible for the generation of pro-invasive exosomes. Furthermore, while RAB27A loss did not alter the number of exosomes secreted, it did change exosome size and altered the composition and abundance of exosomal proteins, some of which are known to regulate cancer cell movement. Our data suggest that RAB27A promotes the biogenesis of a distinct pro-invasive exosome population. These findings support RAB27A as a key cancer regulator, as well as a potential prognostic marker and therapeutic target in melanoma.

Introduction:

Recent therapeutic breakthroughs dramatically improved survival of advanced melanoma patients, although problems with primary and acquired drug resistance and toxicity still remain[1]. Improved understanding of the cellular and molecular cues driving melanoma metastasis and progression will likely identify novel druggable targets which ultimately may be utilized to prevent disease progression and improve patient survival.

The RAB GTPase family (>60 members) regulates many steps in intracellular vesicular trafficking such as budding, movement, tethering, docking and fusion. RABs mediate trafficking of proteins and organelles involved in cell growth, survival and motility. Given these important functions, RABs have become a critical focus among cancer progression regulators[2]. RAB27A is expressed in a subset of specialized secretory cell types, and functions as a complex with the RAB27A-specific effector melanophilin and the motor protein myosin-Va to regulate melanosome trafficking in melanocytes[3, 4]. *RAB27A* expression is regulated by microphthalmia-associated transcription factor (MITF), an oncogene amplified in approximately 10-20% of melanomas and associated with decreased patient survival[5, 6]. Copy number and gene expression data in early passage melanoma cell lines identified *RAB27A* as a "driver" gene that promotes melanoma cell proliferation[7]. RAB27A has also been linked to exosome secretion and education of bone marrow progenitor cells to create a metastatic niche[8]. Exosomes are a well-known driver of cancer progression, and can influence cancer and non-cancer cell types. Notably, exosomes have recently been implicated in immunosuppression via the presence of PD-L1 on the surface of melanoma exosomes[9].

The exact functions of RAB27A in melanoma biology, exosome biogenesis/secretion and disease progression remain ill-defined. Here, we investigated the expression of RAB27A in clinical melanoma samples and the function of RAB27A in melanoma cell lines. *RAB27A* was overexpressed in a subset of melanomas, and high gene and protein expression correlated with poor survival in melanoma patients. Furthermore, RAB27A promoted secretion of a distinct population of pro-invasive exosomes, and enhanced melanoma cell motility, invasion and metastasis. Together, our data demonstrate that RAB27A plays an integral role in melanoma cell invasion and metastasis via regulation of exosome biogenesis.

Materials and Methods:

Melanoma patient samples and RAB27A immunohistochemistry. Archival tissue pathology specimens identified from the Melanoma Institute Australia (MIA) Research Database as matching fresh-frozen tissue specimens banked by the MIA Biobank and included in The Cancer Genome Atlas (TCGA) project were utilized (n=95, from which 63 patients had sufficient tumor tissue for evaluation of RAB27A staining). Criteria for inclusion of MIA patients in the TCGA project were AJCC stage III (n=55) or stage IV (n=8) at time of collection from and follow-up data were retrieved from the MIA Research Database.

Tissue microarray construction, processing and immunohistochemical staining is described in Supplementary Methods. Assessment of RAB27A protein expression was undertaken using an intensity score of 0-3. All immunohistochemistry (IHC) slides were independently reviewed (LAJ & RAS) and a consensus was reached on discrepant cases.

Differentially expressed gene analysis and gene set enrichment. RNAseq data (n=63; samples submitted to the TCGA by the MIA) were retrieved from the TCGA Data Portal for melanoma samples that matched the same tumor the IHC staining was performed on. The sequencing files were processed, normalized and visualized using R packages, 'Rsubread' and 'edgeR', within OmicsOffice Pro version 6 (PerkinElmer)[10]. Briefly, the reads were aligned to the UCSC hg19 reference genome. Subsequently, data were summarized to reads count matrix representing the gene level expression using featureCounts function. These summarized gene values were normalized to fragments per kilobase million (FPKM) values[11]. RAB27A high and low groups were assigned based on IHC staining, and differentially expressed genes were identified as those with a p-value of <0.05 with Benjamini-Hochberg (BH) multiple testing correction at 5% false-discovery rate (FDR). Differentially expressed genes were annotated to cellular components (UniprotIDs) followed by Gene Ontology enrichment analysis using hypergeometric distribution model and FDR threshold of 0.05 to obtain significant results.

Cell lines. The human melanoma cell lines C8161, 1205Lu, WM793, WM983B, WM983C, WM164 and 451Lu were genotypically characterized[12-14] and grown as described[15]. All human melanoma cell lines and HEK293T were authenticated by STR fingerprinting (Molecular Genetics facility, Garvan Institute of Medical Research, Darlinghurst, NSW, Australia). B16-F10 melanoma cells were obtained from ATCC. WM164 cells stably expressing Fluorescence Ubiquitination Cell Cycle Indicator (FUCCI) were created as previously described[15, 16]. Cells were tested for mycoplasma using DAPI staining and high-magnification microscopy, as well as PCR at Cell Bank Australia.

3D melanoma spheroid assay. Melanoma spheroids were prepared as described previously[15, 17, 18]. At least three spheroids were implanted into collagen per condition, experiments were repeated at least three times. Spheroids were imaged using a Nikon Inverted Microscope (4× Plan Fluor objective NA 0.13) and blinded manual invasion measurements (distance from the edge of the spheroid to the invading cell front – three distances taken per spheroid) were performed using Volocity software (Perkin Elmer).

Mouse metastasis model. Mouse work was approved by the Sydney Local Health District Animal Ethics Committee. B16-F10 cells were resuspended in culture medium at 4×10^7 cells/ml. Immediately prior to injection, the cell suspension was diluted 1:1 with Matrigel (BD Biosciences). The cell/Matrigel suspension (25 μl) was injected intradermally into the ears of WB6 mice (5×10^5 cells/mouse). Tumor size was measured using digital Vernier calipers and calculated using the formula: Volume = $(\text{width})^2 \times \text{length}/2$. Health was assessed by monitoring behavior, weight, and tumor appearance. Upon sacrifice 9-13 days post-injection (when tumors reached approximately 500 mm^3), the draining retroauricular lymph nodes and corresponding control lymph nodes from the uninjected ear were harvested in PBS, fixed in formalin and examined for visible (black) metastases using a Leica M205 FA stereomicroscope (Leica Plan APO 1.0× objective).

Exosome purification. WM164 and WM983C cells were cultured in medium supplemented with 1% exosome-depleted FBS (Exo-FBS, System Biosciences). B16-F10 cells were cultured in medium supplemented with 10% exosome-depleted FBS (HyClone FBS, GE lifesciences, with bovine exosomes depleted by ultracentrifugation at 100,000 × g for 18 h). Conditioned medium was collected from

48h cell cultures, centrifuged at 300 × g for 10 min to remove floating cells and then centrifuged again at 20,000 × g for 35 min. Exosomes were then collected by ultracentrifugation of the supernatant at 100,000 × g for 70 min. The exosome pellets were resuspended in 12 ml of PBS and harvested by centrifugation at 100,000 × g for a further 70 min.

Although we acknowledge a recent position description from the International Society for Extracellular Vesicles that indicates current methods are not sufficient to identify exosomes as opposed to other EVs[19], we use the term "exosome" to describe the extracellular vesicles (EVs) derived from our melanoma cells. Our EVs are positive for proteins commonly found in exosome preparations, are negative for proteins not expected in exosomes and conform to the size range commonly described for exosomes[20]. The methods we use to purify and characterise our extracellular vesicles are consistent with the methods suggested as the minimal experimental requirements to claim the presence of extracellular vesicles[19].

Proteomic analysis. Exosomal proteomics was performed by reverse-phase high-pressure liquid chromatography mass spectrometry. Detailed protocols are described in Supplementary Methods. Proteins with significantly higher abundance in the control exosomes were analyzed by IPA (Ingenuity Pathway Analysis, QIAGEN bioinformatics) using the accession ID and normalized abundance counting.

Further details on materials and methods can be found in Supplementary Methods.

Results:

***RAB27A* is overexpressed in melanoma compared to benign nevi, and is associated with decreased patient survival.**

To compare the expression of *RAB27A* in normal skin, benign nevi and melanoma, we analyzed publicly-available microarray data *in silico* (Gene Expression Omnibus; GDS1375)[21]. *RAB27A* was upregulated in melanomas relative to nevi or normal skin, although *RAB27A* expression levels between individual melanoma samples were highly variable (Figure 1A). In another publicly available dataset we observed an upregulation of *RAB27A* mRNA levels with increasing stages of melanoma progression (Gene Expression Omnibus; GDS1989[22]; Supplementary Figure S1A). RAB27A protein was detected via Western blotting in all metastatic melanoma cell lines tested, with high expression in 1205Lu, WM983B, WM983C, WM164 and 451Lu (Figure 1B).

To determine if *RAB27A* expression was associated with melanoma patient outcomes, we analyzed TCGA gene expression data[23]. High *RAB27A* mRNA expression (top 20% of samples) was associated with decreased melanoma-specific survival in stage III melanoma patients compared to those with low levels of *RAB27A* (bottom 20% of samples; Figure 1C, Supplementary Figure S1B). To confirm the association of RAB27A expression with reduced survival at the protein level, we performed immunohistochemistry (IHC) of RAB27A in a subset of the same TCGA samples. Melanomas showed a range of RAB27A staining graded as 0 (none) to 3 (high) for intensity (Figure 1D). RAB27A typically showed granular staining within the cytoplasm of melanoma cells (Supplementary Figure S1C). The moderate/high RAB27A (intensity 2-3) stage III melanoma samples again showed decreased

melanoma-specific survival compared to negative/low (intensity 0-1) samples, although this association did not reach significance (Log Rank p=0.084; Figure 1E). This may be due to the smaller number of samples that were suitable for staining (n=63) compared to the number of samples available for gene expression analysis (n=170).

High RAB27A protein expression is associated with enriched expression of melanosome, exosome and exocytic vesicle associated genes in melanoma

RAB27A protein intensity correlated with the *RAB27A* RNA expression level of the same TCGA samples as expected (r=0.21, p=0.000134). Further differential expression analysis grouped samples based on RAB27A medium/high vs. the negative/low IHC intensity. Differential expression (DE) analysis identified 177 DE genes between RAB27A-high and -low melanoma samples (Figure 1F). Functional enrichment analysis of the DE genes (FDR 0.05, min genes n=3) identified higher expression of gene ontology cellular components associated with melanosomes, lysosomes, exosomes and exocytic vesicles in RAB27A IHC-positive melanomas (Figure 1G, Supplementary Figure S1D). Pathway analysis identified enriched expression of genes involved in cell movement, cell-to-cell signaling/protein trafficking, cell morphology, lipid and carbohydrate metabolism, protein synthesis and degradation, and cell cycle in RAB27A-positive melanoma (Supplementary Fig S1E). IHC and gene expression data thus suggest that RAB27A correlates negatively with survival and is associated with genes that are involved in cancer promoting cellular functions and the exosome/secretory pathway.

***RAB27A*-knockdown in RAB27A-high melanoma cell lines decreases spheroid invasion and cell motility in 3D.**

To determine the biological role of RAB27A in melanoma, *RAB27A* was knocked down in the RAB27A-high cell lines WM164, WM983C and 1205Lu using lentiviral shRNA constructs. Western blotting confirmed substantial reduction of RAB27A protein levels (Figure 2A, Supplementary Figures S2B-C). To study invasion, we utilized a 3D melanoma spheroid model that mimics *in vivo* tumor architecture and microenvironment[15]. *RAB27A*-knockdown (KD) in these RAB27A-high cell lines resulted in strongly reduced invasion into the collagen matrix using three effective *RAB27A* shRNAs (sh#1, sh#2, sh#4; Figure 2B, 2C, Supplementary Figure S2A, S2D), whereas a less effective *RAB27A* shRNA (sh#3; Supplementary Figure S2A-B) did not impair invasion. In contrast to the RAB27A-high cell lines, *RAB27A*-KD in the RAB27A-low cell line C8161 did not reduce spheroid invasion (Supplementary Figure S2C-E), indicating that this melanoma cell line is not dependent on RAB27A for invasion.

To determine the effect of *RAB27A*-KD on cell motility, cells were embedded in low density into 3D collagen matrix and tracked *via* live-imaging. In WM164 and WM983C, *RAB27A*-KD significantly reduced cell speed (Figure 2D). Although slower moving, *RAB27A*-KD cells still retained an ability to form long thin membrane projections into the matrix (Supplementary Movies S1, S2). To determine if changes in matrix metalloproteinases secreted into the medium were involved in the *RAB27A*-KD invasion phenotype in RAB27A-high cell lines, we performed gelatin zymography on conditioned medium from WM164 control and *RAB27A*-KD cell lines. No changes in zymography bands were seen (Supplementary Figure S2F),

indicating that secreted gelatinases, likely MMP-2 and MMP-9, are not involved in the RAB27A-mediated invasion phenotype. Adhesion to collagen matrix was also not significantly altered by *RAB27A*-KD in WM164 (Supplementary Figure S2G), indicating that changes in collagen binding molecules are not involved in the *RAB27A*-KD invasion defect.

RAB27A co-localizes with melanosome and multivesicular body/exosome markers in melanoma cell lines and exosomes/melanosomes are secreted from B16-F10 melanoma cells.

To gain more insight into the function of RAB27A in melanoma cells, we investigated the intracellular localization using transient transfection of EGFP-tagged RAB27A. GFP-RAB fusion proteins including GFP-RAB27A have been shown to localize correctly to target membranes in melanocytic and other cell types[3, 24]. Immunofluorescence using an antibody to RAB27A showed co-localization with GFP-RAB27A expression (Supplementary Figure S3A), confirming the correct exogenous expression of RAB27A. Although a small amount of endogenous RAB27A was detected in melanoma cells, the signal was too weak to be used for co-localization studies. Our human cell lines are hypopigmented, however, GFP-RAB27A showed strong co-localization with melanosome marker Ta99 (Tyrosinase related protein 1, TYRP1) in WM983C (Figure 3A). WM164 did not express TYRP1, but there was partial co-localization of GFP-RAB27A with the melanosome marker HMB45 in both cell lines (g100 or pmel17, marker for stage II-III melanosomes; Supplementary Figure S3B-C). The exosome/late endosome/multivesicular body (MVB) marker CD63 co-localized with GFP-RAB27A in both WM983C and WM164, similar to the melanosome marker Ta99 (Figure 3B, Supplementary Figure

S3D-E). In contrast, there was an inverse correlation of GFP-RAB27A with the DAPI DNA stain (Supplementary Figure S3E), and only a small amount of co-localization with the lysosome marker LAMP-1 and the recycling endosome markers mCherry-Rab11a or internalized transferrin (Supplementary Figure S3F-H).

CD63 and LAMP1 have been found in or associated with the melanosome[25, 26], and TYRP1 has also been found in melanoma exosomes[8]. Given this potential marker overlap and the fact that our human melanoma cell lines do not contain mature melanosomes, it is difficult to accurately distinguish immature melanosomes, late endosomes/MVBs or lysosomes using these markers. Therefore, we investigated the localization of GFP-RAB27A in pigmented B16-F10 mouse melanoma cells. Both GFP-RAB27A and partially GFP-CD63 (Figure 3D) co-localized with mature melanosomes and the melanosome marker HMB45 (Supplementary Figure S3I-J).

To investigate the relationship between melanosomes, MVBs and exosomes in melanoma cells in more detail, we performed TEM on B16-F10 cells. We have previously shown via TEM that various stages of melanosome maturation in melanoma cells and melanocytes can readily be differentiated from other organelles[3, 27]. Black mature melanin-filled melanosomes were found either singly, or inside larger MVBs (Figure 3E). Smaller MVBs without melanin were also common. Melanin-filled melanosomes often appeared granular. Granular melanosomes have previously been described in melanoma cell lines (reviewed in[28]). Notably, extracellular vesicles of ~100 nm in size (exosomes) and granular melanosomes often appeared to be secreted together at the plasma membrane, suggesting a common secretory pathway.

RAB27A loss does not alter CD63$^+$ MVB size, localization or number in melanoma cells.

Given the co-localization of RAB27A with the exosome/MVB marker CD63, and the fact that RAB27 has been proposed to regulate MVB size/docking in HeLa cells[29], we investigated the distribution of CD63 in WM983C and WM164 *RAB27A*-KD cells *via* immunofluorescence. No obvious changes in the distribution or size of CD63-positive structures were seen (Supplementary Figure S4A-B). There was also no change in the total amount of CD63 present in *RAB27A*-KD cells quantified by flow cytometry (Supplementary Figure S4C).

To better clarify the effect of loss of RAB27A on melanosomes versus MVBs, *RAB27A* was knocked out from pigmented B16-F10 cells by CRISPR-Cas9. Single cell *RAB27A*-CRISPR clones were generated and Western blotting confirmed the complete loss of RAB27A (Figure 4A). Contrary to a previous report that loss of RAB27A resulted in an increase in MVB size in HeLa cells[29], *RAB27A*-knockout did not increase MVB diameter in B16-F10 cells visualized *via* TEM (Supplementary Figure S4D). Ostrowski and colleagues measured CD63$^+$ MVBs, while here we have measured any MVB with intraluminal vesicles. Similar to human *RAB27A*-KD cells, B16-F10 CRISPR *RAB27A*-KO cells showed no change in total CD63 exosome/MVB marker intensity via flow cytometry (Supplementary Figure S4E), indicating that loss of RAB27A does not cause accumulation of CD63$^+$ MVBs within melanoma cells.

CRISPR-knockout of *Rab27a* in B16-F10 mouse metastatic melanoma cells reduces melanoma cell motility *in vitro* and spontaneous metastasis *in vivo*.

To confirm that loss of Rab27a in B16-F10 melanoma cells also impaired invasion *in vitro*, we used live-cell imaging to track cell motility in collagen matrix. Similar to *RAB27A*-knockdown in human melanoma cell lines, B16-F10 CRISPR *Rab27a*-knockout (KO) cells showed impaired motility in collagen (Figure 4B). B16-F10 cells did not readily form spheroids therefore spheroid invasion was not tested.

B16-F10 cell tumors reliably form lymphatic metastases in mice[30]. To confirm that loss of Rab27a inhibits spontaneous melanoma metastasis *in vivo*, we injected B16-F10 vector control or CRISPR *Rab27a*-KO cells intra-dermally into the ears of C57B1/6 mice. Loss of Rab27a did not alter tumor growth (Figure 4C). Approximately 9-13 days post-injection, mice were euthanized and the tumor-draining lymph nodes were analyzed for metastasis. Lymphatic metastases were determined by the observation of a pigmented mass (Figure 4D). B16-F10 CRISPR *Rab27a*-KO clone tumor-bearing mice showed a marked decrease in metastasis compared to B16-F10 wild type and vector control tumors (Figure 4E), indicating that Rab27a promotes melanoma metastasis.

RAB27A-knockdown invasion phenotype can be partially rescued by exosomes in RAB27A replete cell conditioned medium.

Given the correlation of RAB27A expression with exosome and exocytic vesicle genes (Supplementary Figure S1D), and the previously described role of RAB27A in exosome secretion and the secretory pathway, we investigated whether secreted factors in conditioned medium played a role in the invasion and motility phenotypes observed in *RAB27A*-KD cells. The invasion defects of WM164 and WM983C *RAB27A*-KD spheroids were partially rescued by culturing in conditioned medium

from control cells (Figure 5A-B). Moreover, conditioned medium from WM164 or WM983 control cells rescued the reduced motility of *RAB27A*-KD cells in collagen (Figure 5C). These data indicate that secreted factors in the conditioned medium are involved in RAB27A-mediated invasion and motility of melanoma cells.

To determine if exosomes were involved in the rescue of *RAB27A*-KD cell invasion with conditioned medium, WM164 control or *RAB27A*-KD cell conditioned medium was depleted of exosomes and other secreted vesicles via ultracentrifugation (at 100,000g). Supernatant of the ultracentrifuged conditioned medium from WM164 control cells was cultured with WM164 *RAB27A*-KD spheroids and the rescue of the *RAB27A*-KD cell invasion was no longer observed (Figure 5D). This suggests exosomes or other secreted vesicles are involved in the invasion defect caused by *RAB27A* knockdown.

To confirm the role of exosomes in the *RAB27A*-KD invasion rescue by conditioned medium, purified exosomes from control WM164 cells were resuspended in exosome depleted medium and added to WM164 *RAB27A*-KD spheroids. Similar to conditioned medium, a partial rescue of the invasion phenotype in *RAB27A*-KD spheroids was observed after addition of exosomes purified from control cells (Figure 5E). In contrast, exosomes purified from *RAB27A*-KD cells could not rescue the *RAB27A*-KD invasion defect (Figure 5E). To demonstrate cell line-independent contribution of exosomes in RAB27A-regulated melanoma invasion, exosomes purified from control and *RAB27A*-KD WM164 cells were added to intrinsically RAB27A-low WM793 spheroids. Exosomes secreted by WM164 control cells dramatically increased WM793 invasion compared to *RAB27A*-KD WM164

exosomes or the PBS only negative control (Figure 5F and 5G). Therefore, exosomes are strongly indicated to play a crucial role in RAB27A-mediated melanoma invasion.

Loss of RAB27A does not alter the total protein level or number of exosomes secreted from melanoma cells, but does alter exosome protein composition and morphology.

Previous studies have indicated that loss of RAB27A causes reduction of secreted exosomes from various cell types including melanoma cell lines[8, 29, 31]. To investigate if *RAB27A* knockdown influenced the number of secreted exosomes, we utilized NanoSight nanoparticle tracking and BCA protein assay to quantify the number and total protein levels of purified exosomes secreted from the same number of melanoma control or *RAB27A*-KD/KO cells. NanoSight measurements revealed purified exosomes were in the expected size range of around 100-200 nm (Supplementary Figure S5A). Western blotting of known exosome markers (CD9, TSG101, CD63; Figure 6A) and non-exosome negative control markers (GAPDH, Calnexin, GM130; Supplementary Figure S5B) confirmed the purity of our exosome samples.

NanoSight and BCA measurements revealed no difference in the total number and total protein content of secreted exosomes after *RAB27A*-KD in WM164 and WM983C cells or *Rab27a* CRISPR-KO in B16-F10 cells (Figure 6B-C, Supplementary Figure S5C). To support this finding, we also performed siRNA-knockdown of *Rab27a* in B16-F10 cells. Western blot analysis confirmed the reduction of Rab27a (Supplementary Figure S5D). Consistent with shRNA and CRISPR-KO, siRNA-knockdown of *Rab27a* did not decrease the number of secreted exosomes in B16-F10 melanoma cells (Supplementary Figure S5E). In contrast to

previous reports, our data suggest that Rab27a loss does not decrease exosome secretion in melanoma.

To investigate whether exosome protein composition was altered by loss of RAB27A, exosome-specific protein levels found in exosomes isolated from the same number of control or *RAB27A*-KD melanoma cells were quantified through Western blotting. BCA assay confirmed similar amounts of total protein in the control and *RAB27A*-KD exosome samples (Figure 6C). In support of the co-localization studies, Western blotting confirmed that RAB27A protein is associated with purified exosomes in WM164 and B16-F10 melanoma cells, while RAB27A was not detected in exosomes from *RAB27A*-KD or CRISPR-KO cells, as expected (Figure 6A). A reduction of CD9 and an increase of TSG101 and CD63 were observed in the exosomes from WM164 *RAB27A*-KD and B16-F10 *Rab27a* CRISPR-KO cells compared to the control cells (Figure 6A). Notably, TEM of purified exosomes from WM164 cells showed an altered morphology after *RAB27A*-KD, with an increase in smaller exosomes (<100nm; Figure 6D-F). Although NanoSight did not detect changes in exosome size, this may be due to a lower sensitivity in measuring exosomes <100nm. To further investigate the alteration in exosome populations, IEM of CD63 on purified exosomes from WM164 cells was carried out. IEM indicated that the CD63-enriched exosome population was smaller than the $CD63^-$ population and was increased after *RAB27A*-KD (Figure 6G-I). This is consistent with the Western blotting data showing that CD63 is increased in *RAB27A*-KD exosomes (Figure 6A). These data suggest that while loss of RAB27A does not alter the number of exosomes secreted from melanoma cells, it does change distinct populations of exosomes.

Proteomics analysis identifies changes in exosome proteins involved in cell movement after *RAB27A* knockdown in melanoma cells

To investigate the changes in exosome proteins caused by loss of RAB27A, exosomes secreted by WM164 non-target control and shRNA#1 *RAB27A*-KD cells were analyzed by label-free quantitative mass spectrometry. Biological triplicates were analyzed within each group and samples within each group clustered separately from samples in other groups (Supplementary Figure S6A). A total of 2187 proteins were identified across the exosome samples, 1994 of which were common to control and RAB27A-knockdown exosomes (Figure 6J). Of the proteins that were found in both samples, 103 were downregulated in knockdown exosomes and 250 were upregulated (Figure 6J, Supplementary Figure S6B). Consistent with our Western blotting results, RAB27A was lower and TSG101 higher in RAB27A-knockdown exosomes, confirming that there are differences in the abundance of exosome-specific proteins in exosomes secreted by RAB27A-deficient cells. CD63 was also higher in knockdown exosomes although the difference was not statistically significant (Supplementary Figure S6C). Of note, several RABs were enriched in exosomes after *RAB27A*-KD (Supplementary Figure S6D). These RABs may be involved in RAB27A-independent secretion of exosomes in melanoma cells. Especially RAB11 (including RAB11A and RAB11B; Supplementary Figure S6D), which has been implicated in regulating $CD63^+$ exosome release[32]. The increase of RAB11 in KD exosomes was validated by Western blotting (Supplementary Figure S6E).

To evaluate the functions of exosomal proteins associated with RAB27A function, we mapped the proteins that were only found in or of significantly higher abundance in the control exosomes to molecular pathways using Ingenuity Pathway Analysis (IPA,

QIAGEN Bioinformatics; Supplementary Table S1). Notably, the top molecular and cellular function identified was cellular movement, and the top networks identified included molecular transport, cellular movement, and cancer (Figure 6K). Proteins only detected or higher in control exosomes (Supplementary Table S1) that have previously been implicated in melanoma cell migration, invasion and metastasis include glypican 1 (GPC1)[33] and EPH receptor B4 (EPHB4[34]; Supplementary Figure S6F) and plasminogen activator, tissue type (PLAT; Supplementary Table S1)[35]. The decrease of GPC1 in KD exosomes was validated by Western blotting (Supplementary Figure S6G). Analysis of gene ontology (GO)/Kyoto Encyclopedia of Genes and Genomes (KEGG) terms also indicated that RAB27A-replete exosomes are enriched for "extracellular matrix", "Extracellular Matrix Disassembly", "SRP-dependant co-translation targeting to the membrane" and "Ribosome". While RAB27A-KD exosomes are selectively enriched for "small GTPase superfamily", "recycling endosome" and "ESCRTIII/ESCRTI" (Supplementary Figure S6H, Supplementary Table S2).

The identified protein changes support our other data indicating that RAB27A promotes biogenesis and/or secretion of a distinct population of exosomes that enhance melanoma cell motility and invasion.

Discussion:

In this study, we have demonstrated that RAB27A is highly expressed in a subset of melanomas, and this high expression is associated with decreased survival in stage III melanoma patients. We show that RAB27A promotes 3D spheroid invasion and motility *in vitro* and metastasis *in vivo* in metastatic melanoma cell lines that highly express this protein. While RAB27A has previously been shown to promote

melanoma metastasis in a mouse model[8], this was proposed to be due to 'education' of bone marrow progenitor cells via RAB27A-dependent melanoma exosomes circulating in the blood and the creation of a metastatic niche. Exosome-educated bone marrow progenitor cells were shown to promote the creation of a metastatic niche. Here we demonstrate a direct role for RAB27A-dependent exosomes in promoting melanoma metastasis through paracrine or autocrine effects on melanoma cell motility and invasion.

Our *in vitro* conditioned medium and purified exosome experiments indicate that RAB27A regulates the biogenesis of a distinct population of exosomes that promote melanoma cell invasion. The enriched expression of exosome-related genes in RAB27A-high clinical melanoma samples, as well as our data showing that RAB27A is present in melanoma exosomes, also supports a role for RAB27A in exosome regulation. Notably, melanoma cell lines producing high concentrations of exosomes have previously been shown to express relatively high levels of *RAB27A*[8].

Individual cells may produce functionally different populations of exosomes, depending on the pathways involved in exosome biogenesis (e.g. origin of endosomes/plasma membrane domains/trafficking proteins). Intracellular trafficking proteins regulate exosome biogenesis and secretion via several different mechanisms, such as targeting of cargo proteins to MVBs, which are the site of exosome generation, and targeting and fusion of MVBs to the plasma membrane for exosome secretion[36]. RAB27A has been linked to docking of $CD63^+$ MVBs with the plasma membrane in HeLa cells[29]. Loss of RAB27A was shown to decrease exosome secretion in melanoma cells[8] and other cell types (bladder carcinoma[37], squamous cell

carcinoma[38], breast cancer[31], HeLa[29]). Surprisingly, we saw no decrease in the number of exosomes secreted, but we did see changes in both the morphology and protein content of exosomes after RAB27A loss. To support our results, we have used two different methods to quantify exosomes and multiple methods of RAB27A-knockdown or -knockout in three different melanoma cell lines. Moreover, changes in exosome proteins and exosome size have been seen previously after RAB27A inhibition in 4T1 breast cancer cells[39].

We hypothesize that in melanoma cells, RAB27A drives secretion of a larger pro-invasive exosome population, characterized by high levels of CD9 and low levels of CD63/TSG101, while smaller CD63/TSG101-high melanoma exosomes are not pro-invasive and are secreted *via* RAB27A-independent mechanisms. Notably, CD9 has been shown to be involved in mechanisms of exosome biogenesis independent of ESCRT (endosomal sorting complex required for transport)[40, 41] while CD63 and TSG101 are involved in ESCRT-dependent exosome biogenesis[42]. Additionally, in RAB27A-KD exosomes we have discovered an upregulation of "ESCRT" GO terms and several syntenin and syndecan members (Supplementary Table S3), which are known to regulate ESCRT-dependent exosome biogenesis[43]. Proteomics analysis also identified an upregulation in RAB22A and RAB11 in *RAB27A*-KD exosomes, both of which have been implicated in exosome secretion previously[44, 45]. RAB11 has also been suggested to be required in $CD63^+$ exosome release[32]. This may indicate a role for these RABs in an alternative, ESCRT-dependent exosome secretory pathway that is upregulated in the absence of RAB27A. Collectively, our data indicate that exosome biogenesis/trafficking may occur via different pathways in melanoma cells, only one of which is dependent on RAB27A; i.e. RAB27A drives secretion of pro-invasive exosomes independent of ESCRT, while RAB27A-KD exosomes work in an

ESCRT- and possibly RAB11/RAB22A-dependent mechanism of exosome biogenesis.

Exosomes have been linked previously to invasion and progression of various cancers (reviewed in[46]). Our data indicate that the cause of the pro-invasive effects of RAB27A-replete exosomes vs. exosomes secreted *via* RAB27A-independent means may be related to changes in exosome populations and their protein cargo. Pathway analysis of proteomic data revealed that the top cellular function associated with RAB27A-replete exosomes was cellular movement, and several proteins previously associated with cancer cell migration, invasion or metastasis were significantly higher in RAB27A-replete exosomes. In particular, EPHB4 is a tyrosine kinase receptor that has been found in cancer exosomes[47] which promotes the migration of melanoma cells through RHO-mediated cytoskeletal reorganization[34], and mediates site specific metastasis *via* adhesive interaction between melanoma and endothelial cells[48]. GPC1 is a cell surface protein known to be enriched in cancer exosomes[49], and is required for efficient metastasis of B16-F10 melanoma *in vivo*[33]. Proteins involved in modulating the extracellular matrix may also be involved in the pro-invasive action of RAB27A-replete exosomes, as gene ontology terms related to "extracellular matrix" and "extracellular matrix disassembly" were enriched in the proteomic analysis. For example, BMP-1 is a metalloprotease that has been linked to cancer metastasis and TGF-β activation[50]; TGF-β has a known role in melanoma migration and dissemination[51].

RAB GTPases are increasingly being implicated in cancer progression in many different cancer types[52]. Most notably, RAB7 has been linked to a lineage-specific tumor dependency in melanoma[53]. In contrast to RAB27A, RAB7 expression is not

regulated by MITF and high RAB7 expression was linked to a decrease in invasiveness and an increase in patient survival. Our data and the previous study by Akavia and co-workers[7] indicate that RAB27A tumor dependency only occurs in melanomas with relatively high levels of RAB27A expression. RAB27A tumor-dependency may also be largely restricted to melanoma, given that RAB27A protein has been shown to be enriched in melanoma compared to other cancer types, both in cell lines[53] and patient tissue[54]. However, studies have also implicated RAB27A in colon cancer[55], breast cancer[31, 56], glioma[57], pancreatic cancer[58], hepatocellular carcinoma[59] and bladder cancer[60]. Here we have highlighted the role of RAB27A in promoting exosome-mediated invasion and metastasis in melanoma. Our data, along with previous studies, suggest that RAB27A may play multiple roles in the progression of melanoma, and may be a novel therapeutic target and/or prognostic factor.

Conflict of interest

John F. Thompson has received honorary and travel support relating to Advisory Board membership for: Provectus Inc, GlaxoSmithKline, BMS Australia, MSD Australia and Roche Australia.

Richard A. Scolyer is a member of Advisory Board for: Merck Sharp & Dohme, Novartis, Myriad and Neracare.

All the other authors declare no conflict of interest.

Acknowledgements:

We thank Dr. Meenhard Herlyn and Ms. Patricia Brafford, The Wistar Institute, Philadelphia, for providing cell lines, and the Imaging and Flow Cytometry Facility at

the Centenary Institute for outstanding technical support. We thank Dr. Joanna Richmond and Dr. Nicholas Ariotti for technical assistance and use of facilities at the Electron Microscope Unit at UNSW. We thank Ms. Angela Connolly and Dr. Ben Crossett for technical support at the Mass Spectrometry Core Facility at USYD. We thank Dr. Dario Strbenac (University of Sydney) for assistance with the TCGA gene expression analysis. We thank Prof. Peter Hersey at Centenary Institute for intellectual contributions. We thank Dr. Renjing Liu at Centenary Institute for providing pX330-IRES Vector. N.K.H. is a Cameron fellow of the Melanoma and Skin Cancer Research Institute, Australia. K.A.B. was a fellow of Cancer Institute New South Wales (13/ECF/1-39). This work was supported by project grants to K.A.B. (1051996, Priority-driven Collaborative Cancer Research Scheme/Cancer Australia/Cure Cancer Australia Foundation), N.K.H. (RG 13-06, Cancer Council New South Wales; APP1003637 and APP1084893, National Health and Medical Research Council) and J.H./J.S.W. (RG17-04, Cancer Council New South Wales). R.A.S. is supported by an Australian Government NHMRC Practitioner Fellowship. The authors also thank colleagues from Melanoma Institute Australia and Royal Prince Alfred Hospital.

References:

1. Luke JJ, Flaherty KT, Ribas A, Long GV. Targeted agents and immunotherapies: optimizing outcomes in melanoma. *Nat Rev Clin Oncol* 2017;**14**: 463-82.

2. Recchi C, Seabra MC. Novel functions for Rab GTPases in multiple aspects of tumour progression. *Biochemical Society transactions* 2012;**40**: 1398-403.

3. Beaumont KA, Hamilton NA, Moores MT, Brown DL, Ohbayashi N, Cairncross O, Cook AL, Smith AG, Misaki R, Fukuda M, Taguchi T, Sturm RA, et al. The recycling endosome protein Rab17 regulates melanocytic filopodia formation and melanosome trafficking. *Traffic* 2011;**12**: 627-43.

4. Fukuda M, Kuroda TS, Mikoshiba K. Slac2-a/melanophilin, the missing link between Rab27 and myosin Va: implications of a tripartite protein complex

for melanosome transport. *The Journal of biological chemistry* 2002;**277**: 12432-6.

5. Garraway LA, Widlund HR, Rubin MA, Getz G, Berger AJ, Ramaswamy S, Beroukhim R, Milner DA, Granter SR, Du J, Lee C, Wagner SN, et al. Integrative genomic analyses identify MITF as a lineage survival oncogene amplified in malignant melanoma. *Nature* 2005;**436**: 117-22.

6. Ugurel S, Houben R, Schrama D, Voigt H, Zapatka M, Schadendorf D, Bröcker EB, Becker JC. Microphthalmia-associated transcription factor gene amplification in metastatic melanoma is a prognostic marker for patient survival, but not a predictive marker for chemosensitivity and chemotherapy response. *Clinical Cancer Research* 2007;**13**: 6344-50.

7. Akavia UD, Litvin O, Kim J, Sanchez-Garcia F, Kotliar D, Causton HC, Pochanard P, Mozes E, Garraway LA, Pe'er D. An integrated approach to uncover drivers of cancer. *Cell* 2010;**143**: 1005-17.

8. Peinado H, Aleckovic M, Lavotshkin S, Matei I, Costa-Silva B, Moreno-Bueno G, Hergueta-Redondo M, Williams C, Garcia-Santos G, Ghajar C, Nitadori-Hoshino A, Hoffman C, et al. Melanoma exosomes educate bone marrow progenitor cells toward a pro-metastatic phenotype through MET. *Nature medicine* 2012;**18**: 883-91.

9. Chen G, Huang AC, Zhang W, Zhang G, Wu M, Xu W, Yu Z, Yang J, Wang B, Sun H, Xia H, Man Q, et al. Exosomal PD-L1 contributes to immunosuppression and is associated with anti-PD-1 response. *Nature* 2018;**560**: 382.

10. Robinson MD, McCarthy DJ, Smyth GK. edgeR: a Bioconductor package for differential expression analysis of digital gene expression data. *Bioinformatics* 2010;**26**: 139-40.

11. Rahman M, Jackson LK, Johnson WE, Li DY, Bild AH, Piccolo SR. Alternative preprocessing of RNA-Sequencing data in The Cancer Genome Atlas leads to improved analysis results. *Bioinformatics* 2015;**31**: 3666-72.

12. Smalley KS, Contractor R, Haass NK, Kulp AN, Atilla-Gokcumen GE, Williams DS, Bregman H, Flaherty KT, Soengas MS, Meggers E. An organometallic protein kinase inhibitor pharmacologically activates p53 and induces apoptosis in human melanoma cells. *Cancer research* 2007;**67**: 209-17.

13. Davies MA, Stemke-Hale K, Lin E, Tellez C, Deng W, Gopal YN, Woodman SE, Calderone TC, Ju Z, Lazar AJ. Integrated molecular and clinical analysis of AKT activation in metastatic melanoma. *Clinical Cancer Research* 2009;**15**: 7538-46.

14. Smalley K, Contractor R, Haass N, Lee J, Nathanson K, Medina C, Flaherty K, Herlyn M. Ki67 expression levels are a better marker of reduced melanoma growth following MEK inhibitor treatment than phospho-ERK levels. *British journal of cancer* 2007;**96**: 445-9.

15. Spoerri L, Beaumont KA, Anfosso A, Haass NK. Real-Time Cell Cycle Imaging in a 3D Cell Culture Model of Melanoma. *Methods Mol Biol* 2017;**1612**: 401-16.

16. Haass NK, Beaumont KA, Hill DS, Anfosso A, Mrass P, Munoz MA, Kinjyo I, Weninger W. Real-time cell cycle imaging during melanoma growth, invasion, and drug response. *Pigment cell & melanoma research* 2014;**27**: 764-76.

17. Beaumont KA, Anfosso A, Ahmed F, Weninger W, Haass NK. Imaging- and Flow Cytometry-based Analysis of Cell Position and the Cell Cycle in 3D Melanoma Spheroids. *Journal of visualized experiments : JoVE* 2015: e53486.

18. Smalley KS, Lioni M, Noma K, Haass NK, Herlyn M. In vitro three-dimensional tumor microenvironment models for anticancer drug discovery. *Expert opinion on drug discovery* 2008;**3**: 1-10.

19. Lötvall J, Hill AF, Hochberg F, Buzás EI, Di Vizio D, Gardiner C, Gho YS, Kurochkin IV, Mathivanan S, Quesenberry P. Minimal experimental requirements for definition of extracellular vesicles and their functions: a position statement from the International Society for Extracellular Vesicles. *Journal of Extracellular Vesicles* 2014;**3**.

20. Peinado H, Zhang H, Matei IR, Costa-Silva B, Hoshino A, Rodrigues G, Psaila B, Kaplan RN, Bromberg JF, Kang Y. Pre-metastatic niches: organ-specific homes for metastases. *Nature Reviews Cancer* 2017;**17**: 302.

21. Talantov D, Mazumder A, Jack XY, Briggs T, Jiang Y, Backus J, Atkins D, Wang Y. Novel genes associated with malignant melanoma but not benign melanocytic lesions. *Clinical cancer research* 2005;**11**: 7234-42.

22. Smith AP, Hoek K, Becker D. Whole-genome expression profiling of the melanoma progression pathway reveals marked molecular differences between nevi/melanoma in situ and advanced-stage melanomas. *Cancer biology & therapy* 2005;**4**: 1018-29.

23. Akbani R, Akdemir KC, Aksoy BA, Albert M, Ally A, Amin SB, Arachchi H, Arora A, Auman JT, Ayala B. Genomic classification of cutaneous melanoma. *Cell* 2015;**161**: 1681-96.

24. Hume AN, Collinson LM, Rapak A, Gomes AQ, Hopkins CR, Seabra MC. Rab27a regulates the peripheral distribution of melanosomes in melanocytes. *The Journal of cell biology* 2001;**152**: 795-808.

25. Chi A, Valencia J, Hu Z, Watabe H, Yamaguchi H, Mangini N, Huang H, Canfield V, Cheng K, Yang F. Proteomic and bioinformatic characterization of the biogenesis and function of melanosomes. *Journal of proteome research* 2006;**5**: 3135.

26. van Niel G, Charrin S, Simoes S, Romao M, Rochin L, Saftig P, Marks MS, Rubinstein E, Raposo G. The tetraspanin CD63 regulates ESCRT-independent and dependent endosomal sorting during melanogenesis. *Developmental cell* 2011;**21**: 708.

27. Cook AL, Chen W, Thurber AE, Smit DJ, Smith AG, Bladen TG, Brown DL, Duffy DL, Pastorino L, Bianchi-Scarra G, Leonard JH, Stow JL, et al. Analysis of cultured human melanocytes based on polymorphisms within the SLC45A2/MATP, SLC24A5/NCKX5, and OCA2/P loci. *The Journal of investigative dermatology* 2009;**129**: 392-405.

28. Slominski A, Tobin DJ, Shibahara S, Wortsman J. Melanin pigmentation in mammalian skin and its hormonal regulation. *Physiological reviews* 2004;**84**: 1155-228.

29. Ostrowski M, Carmo NB, Krumeich S, Fanget I, Raposo G, Savina A, Moita CF, Schauer K, Hume AN, Freitas RP, Goud B, Benaroch P, et al. Rab27a and Rab27b control different steps of the exosome secretion pathway. *Nature cell biology* 2010;**12**: 19-30; sup pp 1-13.

30. Bobek V, Kolostova K, Pinterova D, Kacprzak G, Adamiak J, Kolodziej J, Boubelik M, Kubecova M, Hoffman RM. A clinically relevant, syngeneic model of spontaneous, highly metastatic B16 mouse melanoma. *Anticancer research* 2010;**30**: 4799-803.

31. Bobrie A, Krumeich S, Reyal F, Recchi C, Moita LF, Seabra MC, Ostrowski M, Thery C. Rab27a supports exosome-dependent and -independent mechanisms that modify the tumor microenvironment and can promote tumor progression. *Cancer research* 2012;**72**: 4920-30.

32. Messenger S, Woo S, Sun Z, Martin T. A Ca2+-stimulated exosome release pathway in cancer cells is regulated by Munc13-4. *The Journal of cell biology* 2018.

33. Aikawa T, Whipple CA, Lopez ME, Gunn J, Young A, Lander AD, Korc M. Glypican-1 modulates the angiogenic and metastatic potential of human and mouse cancer cells. *The Journal of clinical investigation* 2008;**118**: 89-99.

34. Yang N, Pasquale E, Owen L, Ethell I. The EphB4 receptor-tyrosine kinase promotes the migration of melanoma cells through Rho-mediated actin cytoskeleton reorganization. *The Journal of biological chemistry* 2006;**281**: 32574.

35. Meves A, Nikolova E, Heim JB, Squirewell EJ, Cappel MA, Pittelkow MR, Otley CC, Behrendt N, Saunte DM, Lock-Andersen J. Tumor cell adhesion as a risk factor for sentinel lymph node metastasis in primary cutaneous melanoma. *Journal of Clinical Oncology* 2015;**33**: 2509.

36. Palmulli R, van Niel G. To be or not to be... secreted as exosomes, a balance finely tuned by the mechanisms of biogenesis. *Essays in biochemistry* 2018;**62**: 177-91.

37. Ostenfeld MS, Jeppesen DK, Laurberg JR, Boysen AT, Bramsen JB, Primdal-Bengtson B, Hendrix A, Lamy P, Dagnaes-Hansen F, Rasmussen MH, Bui KH, Fristrup N, et al. Cellular disposal of miR23b by RAB27-dependent exosome release is linked to acquisition of metastatic properties. *Cancer research* 2014;**74**: 5758-71.

38. Hoshino D, Kirkbride KC, Costello K, Clark ES, Sinha S, Grega-Larson N, Tyska MJ, Weaver AM. Exosome secretion is enhanced by invadopodia and drives invasive behavior. *Cell reports* 2013;**5**: 1159-68.

39. Bobrie A, Colombo M, Krumeich S, Raposo G, Théry C. Diverse subpopulations of vesicles secreted by different intracellular mechanisms are present in exosome preparations obtained by differential ultracentrifugation. *Journal of Extracellular Vesicles* 2012;**1**.

40. Chairoungdua A, Smith DL, Pochard P, Hull M, Caplan MJ. Exosome release of β-catenin: a novel mechanism that antagonizes Wnt signaling. *The Journal of cell biology* 2010;**190**: 1079-91.

41. Buschow SI, Nolte - 't Hoen EN, Van Niel G, Pols MS, Ten Broeke T, Lauwen M, Ossendorp F, Melief CJ, Raposo G, Wubbolts R. MHC II in dendritic cells is targeted to lysosomes or T cell - induced exosomes via distinct multivesicular body pathways. *Traffic* 2009;**10**: 1528-42.

42. Zöller M. Exosomes in Cancer Disease. *Methods in molecular biology (Clifton, NJ)* 2016;**1381**: 111.

43. Baietti MF, Zhang Z, Mortier E, Melchior A, Degeest G, Geeraerts A, Ivarsson Y, Depoortere F, Coomans C, Vermeiren E. Syndecan–syntenin–ALIX regulates the biogenesis of exosomes. *Nature cell biology* 2012;**14**: 677.

44. Wang T, Gilkes DM, Takano N, Xiang L, Luo W, Bishop CJ, Chaturvedi P, Green JJ, Semenza GL. Hypoxia-inducible factors and RAB22A mediate formation of microvesicles that stimulate breast cancer invasion and metastasis. *Proceedings of the National Academy of Sciences* 2014: 201410041.

45. Savina A, Fader CM, Damiani MT, Colombo MI. Rab11 promotes docking and fusion of multivesicular bodies in a calcium - dependent manner. *Traffic* 2005;**6**: 131-43.

46. Wu K, Xing F, Wu SY, Watabe K. Extracellular vesicles as emerging targets in cancer: Recent development from bench to bedside. *Biochimica et biophysica acta* 2017.

47. Welton JL, Khanna S, Giles PJ, Brennan P, Brewis IA, Staffurth J, Mason MD, Clayton A. Proteomics Analysis of Bladder Cancer Exosomes. *Molecular & Cellular Proteomics: MCP* 2010;**9**: 1324.

48. Héroult M, Schaffner F, Pfaff D, Prahst C, Kirmse R, Kutschera S, Riedel M, Ludwig T, Vajkoczy P, Graeser R. EphB4 promotes site-specific metastatic tumor cell dissemination by interacting with endothelial cell–expressed EphrinB2. *Molecular Cancer Research* 2010: 1541-7786. MCR-09-0453.

49. Melo SA, Luecke LB, Kahlert C, Fernandez AF, Gammon ST, Kaye J, LeBleu VS, Mittendorf EA, Weitz J, Rahbari N. Glypican-1 identifies cancer exosomes and detects early pancreatic cancer. *Nature* 2015;**523**: 177.

50. Wu X, Liu T, Fang O, Leach L, Hu X, Luo Z. miR-194 suppresses metastasis of non-small cell lung cancer through regulating expression of BMP1 and p27 kip1. *Oncogene* 2014;**33**: 1506.

51. Cantelli G, Orgaz JL, Rodriguez-Hernandez I, Karagiannis P, Maiques O, Matias-Guiu X, Nestle FO, Marti RM, Karagiannis SN, Sanz-Moreno V. TGF-β-induced transcription sustains amoeboid melanoma migration and dissemination. *Current biology* 2015;**25**: 2899-914.

52. Qin X, Wang J, Wang X, Liu F, Jiang B, Zhang Y. Targeting Rabs as a novel therapeutic strategy for cancer therapy. *Drug discovery today* 2017;**22**: 1139-47.

53. Alonso-Curbelo D, Riveiro-Falkenbach E, Perez-Guijarro E, Cifdaloz M, Karras P, Osterloh L, Megias D, Canon E, Calvo TG, Olmeda D, Gomez-Lopez G, Grana O, et al. RAB7 controls melanoma progression by exploiting a lineage-specific wiring of the endolysosomal pathway. *Cancer cell* 2014;**26**: 61-76.

54. Uhlen M, Bjorling E, Agaton C, Szigyarto CA, Amini B, Andersen E, Andersson AC, Angelidou P, Asplund A, Asplund C, Berglund L, Bergstrom K, et al. A human protein atlas for normal and cancer tissues based on antibody proteomics. *Molecular & cellular proteomics : MCP* 2005;**4**: 1920-32.

55. Feng F, Jiang Y, Lu H, Lu X, Wang S, Wang L, Wei M, Lu W, Du Z, Ye Z, Yang G, Yuan F, et al. Rab27A mediated by NF-kappaB promotes the stemness of colon cancer cells via up-regulation of cytokine secretion. *Oncotarget* 2016;**7**: 63342-51.

56. Wang JS, Wang FB, Zhang QG, Shen ZZ, Shao ZM. Enhanced expression of Rab27A gene by breast cancer cells promoting invasiveness and the metastasis potential by secretion of insulin-like growth factor-II. *Molecular cancer research : MCR* 2008;**6**: 372-82.

57. Wang H, Zhao Y, Zhang C, Li M, Jiang C, Li Y. Rab27a was identified as a prognostic biomaker by mRNA profiling, correlated with malignant progression and subtype preference in gliomas. *PloS one* 2014;**9**: e89782.

58. Wang Q, Ni Q, Wang X, Zhu H, Wang Z, Huang J. High expression of RAB27A and TP53 in pancreatic cancer predicts poor survival. *Medical oncology (Northwood, London, England)* 2015;**32**: 372.

59. Dong WW, Mou Q, Chen J, Cui JT, Li WM, Xiao WH. Differential expression of Rab27A/B correlates with clinical outcome in hepatocellular carcinoma. *World journal of gastroenterology* 2012;**18**: 1806-13.

60. Liu J, Gong X, Zhu X, Xue D, Liu Y, Wang P. Rab27A overexpression promotes bladder cancer proliferation and chemoresistance through regulation of NF-kappaB signaling. *Oncotarget* 2017;**8**: 75272-83.

Figure Legends:

Figure 1. *RAB27A* is overexpressed in melanoma, associated with decreased patient survival and enriched expression of melanosome, exosome and exocytic vesicle associated genes in melanoma.

A) *RAB27A* expression (probe 222294) in normal skin (n=7), benign nevi (n=18) and melanoma (n=45) samples from the gene expression omnibus dataset GDS1375. Error bars represent the mean ± SEM. ****p≤0.0001.

B) Western blot showing RAB27A in melanoma cell lines. The human embryonic kidney cell line HEK 293T served as a negative control. Representative of at least three independent experiments.

C) Kaplan-Meier survival curves of stage III melanoma patients (TCGA dataset) stratified by *RAB27A* gene expression. The top 20% *RAB27A* expression samples were compared to the bottom 20% expression samples (n=34 patients per group). Survival is measured as the time interval from a patient's initial diagnosis to the date of death. Crosses indicate that patient follow-up data were unavailable after this point.

D) RAB27A immunohistochemistry scoring (0-3); representative images (note that there were no cases with a score of 1).

E) Kaplan-Meier survival curves of stage III melanoma patients (TCGA dataset) stratified by RAB27A protein expression. Patient survival grouped into negative/low (n=47) vs. moderate/high (n=17) RAB27A staining in melanoma tumor cells. Survival is measured as the time interval from a patient's initial

pathologic diagnosis to the date of death. Crosses indicate that patient follow-up data were unavailable after this point.

F) Volcano plot showing fold change and p-values of differentially expressed genes in *RAB27A*-high samples (score 2/3) compared to *RAB27A*-low samples (score 0/1); *RAB27A* itself is highlighted. Fold change is indicated by different colors.

G) Gene Ontology Functional Enrichment analysis was performed according to roles of cellular components. Top cellular components that correlated with RAB27A moderate-highly stained samples are shown.

Figure 2. *RAB27A* knockdown in RAB27A-high melanoma cell lines decreases spheroid invasion and cell motility.

A) Western blots showing the level of RAB27A protein in empty vector control (Vector), non-targeting shRNA control (non-target), *RAB27A*-knockdown cells: shRNA#1 (RAB27A sh1) and *RAB27A* shRNA#2 (RAB27A sh2) . Representative of at least 3 independent experiments.

B) Phase contrast images of WM983C spheroid invasion 72 h after embedding in collagen. Cells express the non-targeting shRNA, *RAB27A* shRNA#1 or *RAB27A* shRNA#2 as indicated. Arrows indicate the distance cells have invaded away from the edge of the spheroid. Scale bars indicate 200μm. Images are representative of seven independent experiments.

C) Quantification of the distance cells have invaded away from the spheroid edge (normalized to the non-targeting shRNA control). Error bars represent the mean ± SEM of at least n=3 independent experiments. Non-targeting control was compared to the other samples via ANOVA and a Dunnett's test.

D) Motility. Dots represent individual cell speed in 3D collagen. Error bars represent the mean ± SEM. Non-targeting control was compared to the other samples via Kruskal-Wallis and Dunn's test. Graphs are representative of at least three independent experiments.

Figure 3. RAB27A co-localizes with melanosome and multivesicular body/exosome markers in melanoma cell lines and exosomes/melanosomes are secreted from B16-F10 melanoma cells.

A) Representative confocal immunofluorescence image (extended focus) of GFP-RAB27A (green) and Ta99 (red) in WM983C cells. Scale bar in larger image = 20μm, scale bar in zoom image = 5μm.

B) Representative confocal immunofluorescence image (extended focus) of GFP-RAB27A (green) and CD63 (red) in WM983C cells. Scale in larger image = 20μm, scale bar in zoom image = 5μm.

C) Representative confocal fluorescence image (extended focus) of GFP-RAB27A (green) and brightfield in B16-F10 cells. Scale bar in image = 20μm.

D) Representative confocal fluorescence image (extended focus) of GFP-CD63 (green) and brightfield in B16-F10 cells. Scale bar in large image = 20μm, scale bar in zoom image = 4μm

E) Transmission electron microscopy image of B16-F10 cells. Arrows indicate multivesicular bodies (Zoom MVBs) or exosome/melanosome secretion (Zoom PM). Scale bars 2 and 0.5 μm, as indicated.

A) to D) Black and white colors have been applied for single channel images and false colors representing the fluorophores of antibodies have been applied for the overlay images.

Figure 4. CRISPR knockout of *RAB27A* in the B16-F10 mouse metastatic melanoma cell line reduces melanoma cell motility *in vitro* and spontaneous metastasis *in vivo.*

A) Western blots showing the level of RAB27A protein in B16-F10 wild type, empty vector control (vector clone), *RAB27A* CRISPR-knockout cells: clones 1, 2 and 3. Representative of at least 3 independent experiments.

B) Dots represent individual cell speed in 3D collagen. Error bars represent the mean ± SEM. B16-F10 empty vector clone cells were compared to other groups via ANOVA and a Dunnett's test. Representative of at least 4 independent experiments.

C) Mean ear tumor volumes for each group of mice post-injection of B16-F10 wild type, empty vector control (vector clone), *RAB27A* CRISPR KO clone 1 (KO clone1), clone 2 (KO clone2) or clone 3 (KO clone3) cells. Error bars represent the mean ± SEM of 8 mice within each group. This growth curve is representative of at least 2 independent experiments.

D) Percentage of positive and negative lymphatic metastases are presented within each indicated group. Results are pooled from mice in 2-3 independent experiments, n=18 for Vector control clone, CRISPR KO clone1 and clone2, n=16 for wild type and CRISPR KO clone 3.

E) Representative bright field color images of positive and negative lymphatic metastasis, scale bar=1mm.

Figure 5. *RAB27A*-knockdown invasion phenotype can be partially rescued by exosomes in RAB27A replete cell conditioned medium.

A) Phase contrast images of WM983C spheroid invasion 72h after embedding in collagen. Cells are expressing the non-targeting control or *RAB27A* shRNA#1 (indicated as non-target or *RAB27A* sh#1) and are cultured in conditioned medium from cells expressing non-targeting shRNA or *RAB27A* shRNA#1 (indicated as non-target medium or sh#1 medium). Arrows indicate the distance cells have invaded away from the edge of the spheroid. Scale bar = 100 μm. Images are representative of 4 independent experiments.

B) Quantification of the distance WM164 or WM983C cells have invaded away from the spheroid edge (normalized to the spheroids expressing non-targeting shRNA (non-target) cultured in conditioned medium from cells expressing non-targeting control vector (non-target con-medium). Error bars represent the mean ± SEM of at least n=4 independent experiments. Each sample was compared to the other samples via One-way ANOVA and Tukey test.

C) Motility. Dots represent individual cell speed in 3D collagen. Error bars represent mean ± SEM. Cells expressing the non-targeting control or *RAB27A* shRNA#1 (indicated as NT or sh#1) were cultured in conditioned medium from cells expressing non-target control vector or *RAB27A* shRNA#1 (indicated as positive of non-target con-medium or sh#1 con-medium, respectively). The figure is representative of at least 4 independent experiments. Each sample was compared to other samples via One-way ANOVA and Tukey test.

D) Quantification of the distance cells have invaded away from the spheroid edge (same normalization as in Figure 5B). Error bars represent the mean ± SEM of 3 independent experiments. Spheroids expressing *RAB27A* shRNA#1 groups were compared to each other via One-way ANOVA and Tukey test. Non-

target exo-dep con-medium indicates conditioned medium from cells expressing non-targeting control with exosome-depletion.

E) Quantification of the distance cells have invaded away from the spheroid edge (same normalization as in Figure 5B). Error bars represent the mean ± SEM of 3 independent experiments. Spheroids expressing *RAB27A* shRNA#1 groups were compared to each other via One-way ANOVA and Tukey test. Exosome depleted medium supplied with purified exosomes secreted from cells expressing non-targeting vector control or *RAB27A* shRNA#1 are indicated as +non-target exosomes or +Sh#1 exosomes, respectively.

F) Phase contrast images of WM793 spheroid invasion 72h after embedding in collagen. Exosome depleted medium supplied with purified exosomes secreted from 5 x 10^6 WM164 cells expressing non-targeting vector control or *RAB27A* shRNA#1. Arrows indicate the distance cells have invaded away from the edge of the spheroid. Scale bars = 200 μm. Images are representative of 3 independent experiments.

G) Quantification of the distance cells have invaded away from the spheroid edge (normalized to Non-target exosomes). Error bars represent the mean ± SEM of 3 independent experiments. Each sample was compared to the other samples via One-way ANOVA and Tukey test.

Figure 6. Loss of *RAB27A* changes exosome protein content and morphology.

A) Western blots showing levels of RAB27A, CD9 and TSG101 and CD63 in purified exosomes (exo) or cell lysates (CL) from B16-F10 and WM164 control or KD/KO cells as indicated. For WM164, separate gels/blots for each marker were run in parallel using the same batch of purified exosomes. For

B16-F10, CD9 and Tsg101 blots are from one batch, and CD63 and Rab27a are from another batch of purified exosomes. Grey line in the B16-F10 blot indicates a lane cropped from the gel. Proteins were extracted from exosomes secreted by 2×10^7 cells or cell lysates of 2×10^6 cells. Representative of at least 3 independent experiments.

B) NanoSight measurement of exosomes secreted by 10^6 WM164 non-target control and *RAB27A* shRNA-KD cells or B16-F10 wild-type, vector control and *Rab27a* CRISPR-KO clone cells. Numbers of exosomes are normalized to the WM164 non-target control or B16-F10 vector control groups. Error bars represent the mean ± SEM (n=5). WM164 non-target control or B16 vector control groups were compared to other groups via One-way ANOVA and a Dunnett's test; ns = not significant.

C) BCA assay measurement of proteins in purified exosomes secreted 10^6 WM164 non-target control and *RAB27A* shRNA-KD cells or B16-F10 vector control and *Rab27a* CRISPR-KO cells. Protein levels of exosomes are normalized to the WM164 non-target control or B16-10 vector control groups. Error bars represent the mean ± SEM (n=3). WM164 non-target control was compared to *RAB27A* shRNA#1 cells via student t test. B16 vector control group was compared to other groups via One-way ANOVA and Dunnett's test; ns = not significant.

D) Transmission electron microscopy images (negative staining) of exosomes secreted by WM164 non-target control (non-target) and *RAB27A* shRNA#1 KD (*RAB27A* sh#1) cells. Scale bar = 200nm. Representative of two independent experiments.

E) Exosome size. Dots represent diameter of individual exosomes secreted by WM164 non-target control (non-target) and *RAB27A* shRNA#1 KD (sh#1) cells, derived from 10 EM images per group. Error bars represent mean ± SEM. Significance was determined by student t test.

F) Size distribution of exosomes from WM164 non-target or *RAB27A* KD cells.

G) Immunogold EM images of CD63 staining on exosomes secreted by WM164 non-target control (non-target) and *RAB27A* shRNA#1 KD (*RAB27A* sh#1) cells (indicated by arrows). Scale bar = 200nm. Representative of two independent experiments.

H) Exosome size. Dots represent diameter of individual exosomes secreted by WM164 non-target control (non-target), *RAB27A* shRNA#1 KD (RAB27A sh#1) cells, diameter of individual CD63-positive exosomes secreted by WM164 non-target control (CD63+ in non-target) and *RAB27A* shRNA#1 KD (CD63+ in sh#1) cells respectively, derived from 20 EM images per group. Error bars represent mean ± SEM. Each group was compared to other groups via One-way ANOVA and Tukey test.

I) Percentages of CD63 positive and negative exosomes are presented within exosomes secreted by WM164 non-target control (non-target), *RAB27A* shRNA#1 KD (RAB27A sh#1) cells. Error bars represent mean of percentages ± SEM from 2 independent experiments with total 20 images per group. Negative controls from two groups were compared via student t test.

J) Differentially expressed proteins. Top: Venn diagram of proteins shared between WM164 non-target control and *RAB27A* shRNA#1 exosomes as well as unique proteins. Bottom: Venn diagram of common proteins in non-vector control and *RAB27A* shRNA#1 exosomes, showing number of proteins with

significantly higher or lower abundance, indicated as control > shRNA#1 or control < shRNA#1, respectively.

K) Top networks and molecular/cellular functions of significant highly abundant exosomal proteins from WM164 non-target control cells compared to *RAB27A* KD.

Supplementary Figure Legends:

Supplementary Figure S1.

A) Expression value of *RAB27A* mRNA from patient samples of normal skin, nevi and different stages of melanoma progression. Error bars indicate mean ± SEM of at least two patients.

B) Distribution plot showing *RAB27A* gene expression levels within stage III melanoma patients. Each dot indicates an individual patient. Dotted lines indicate the top and bottom 20% cut-off.

C) Representative images of RAB27A immunohistochemical staining in patient melanoma sections, magnification as indicated.

D) Genes within the top cellular components associated with RAB27A moderate-high samples.

E) Canonical Pathways, Diseases Associated Pathways, System Development Pathways and general Molecular Cellular Functions were visualized as bar graphs, each bar represents a term, indicates the number of genes with significant change in expression between the RAB27A-high or RAB27A-low group, colour codes the ratio of genes with higher/lower abundance between the RAB27A-high or RAB27A-low group (i.e. green: higher abundance in

RAB27A-high; red: higher abundance in RAB27A-low), and represents the enrichment score as bar length (-log10 FDR).

Supplementary Figure S2.

A) Phase contrast images of WM164 spheroid invasion 72h after embedding in collagen. Cells express the non-targeting shRNA control (non-target), *RAB27A* shRNA#1, *RAB27A* shRNA#2, *RAB27A* shRNA#3 or *RAB27A* shRNA#4 KD cells, as indicated. Arrows indicate the distance cells have invaded away from the edge of the spheroid. Scale bars indicate 200 μm. Images are representative of at least 3 independent experiments.

B) Western blots showing the level of RAB27A protein in non-targeting shRNA control (non-target), *RAB27A*-KD cells: shRNA#1 (27A sh1), *RAB27A* shRNA#2 (27A sh2), *RAB27A* shRNA#3 (27A sh3) and *RAB27A* shRNA#4 (27A sh4). Representative of at least 3 independent experiments.

C) Western blots showing the level of RAB27A protein in 1205Lu and C8161, empty vector control (vector), non-targeting shRNA control, *RAB27A*-KD cells: shRNA#1 (27A sh1) and *RAB27A* shRNA#2 (27A sh2). Representative of at least 3 independent experiments.

D) Quantification of the distance cells have invaded away from the spheroid edge after 72h for 1205Lu and 24 h for C8161 (normalized to the non-targeting shRNA control). Error bars represent the mean ± SEM of n=3 independent experiments. Non-targeting control was compared to the other samples via ANOVA and a Dunnett's test.

E) Phase contrast images of C8161 spheroid invasion 24 h after embedding in collagen. Cells express the non-targeting shRNA, *RAB27A* shRNA#1 or #2 as

indicated. Arrows indicate the distance cells have invaded away from the edge of the spheroid. Images are representative of 3 independent experiments.

F) Gelatin zymography showing the MMP activities in the medium derived from WM164 non-target control and *RAB27A* shRNA#1 KD cells. Representative of at least 3 independent experiments.

G) MTS assay absorbance of WM164 vector control, non-target control, *RAB27A* shRNA#1 KD and *RAB27A* shRNA#2 KD cells that have adhered to collagen after 30 min of incubation (indicated as vector, non-target, sh1 and sh2 accordingly). Empty well control was indicated as No cells. Error bars represent the mean ± SEM of n=4 independent experiments.

Supplementary Figure S3.

A) Representative confocal immunofluorescence image (extended focus) of GFP-RAB27A (green) and RAB27A Ab (red) in WM983C cells. Scale bar = 20 μm.

B) Representative confocal immunofluorescence image (extended focus) of GFP-RAB27A (green) and HMB45 Ab (red) in WM983C cells. Scale bar in larger image = 20 μm. Scale bar in zoom image = 5 μm.

C) Representative confocal immunofluorescence image (extended focus) of GFP-RAB27A (green) and HMB45 Ab (red) in WM164 cells. Scale bar in larger image = 20 μm. Scale bar in zoom image = 5 μm.

D) Representative confocal immunofluorescence image (extended focus) of GFP-RAB27A (green) and CD63 Ab (red) in WM164 cells. Scale bar = 20μm.

E) Quantification of the correlation between the indicated markers using Pearsons correlation analysis. Error bars represent the mean ± SEM of at least n=9 individual cells from 3 independent experiments.

F) Representative confocal immunofluorescence image (extended focus) of GFP-RAB27A (green), mCherry-RAB11A (red) and Alexa647-tagged Transferrin (blue) after 60min uptake in WM164 cells. Scale bar = 20 μm.

G) Representative confocal immunofluorescence image (extended focus) of GFP-RAB27A (green), LAMP1 Ab (red) in WM164 cells. Scale bar = 20 μm.

H) Representative confocal immunofluorescence image (extended focus) of GFP-RAB27A (green), HMB45 Ab (red) and mCherry-RAB11A (blue) in 451Lu cells. Scale bar in larger image = 10 μm. Scale bar in zoom images = 2 μm.

I) Representative confocal immunofluorescence image (extended focus) of GFP-RAB27A (green) and HMB45 Ab (red) in B16-F10 cells. Scale bar = 20 μm.

J) Representative confocal immunofluorescence image (extended focus) of GFP-CD63 (green) and HMB45 Ab (red) in B16F10 cells. Scale bar = 20 μm.

Black and white colors have been applied for single channel images and false colors representing the fluorophores of antibodies have been applied for the overlay images.

Supplementary Figure S4.

A) Representative confocal immunofluorescence image (extended focus) of CD63 Ab in WM983C control (non-target sh) or *RAB27A* shRNA#1 cells. Scale bar = 20 μm.

B) Representative confocal immunofluorescence image (extended focus) of CD63 Ab (white) and DAPI (blue) in WM164 control (non-target) or *RAB27A* shRNA#1 cells. Scale bar = 20 μm.

C) Flow cytometry histogram of total CD63 Ab staining in permeabilized WM164 control or shRNA KD cells.

D) Individual MVB diameter measurements from B16-F10 wild-type, vector or *Rab27a* CRISPR KO cells.

E) Flow cytometry histogram of total CD63 Ab staining in permeabilized B16-F10 wild-type (WT), vector control (vec2), CRISPR *Rab27a* KO clone 1 (KO1) and clone 2 (KO2) cells versus secondary antibody only control (secondary only).

Supplementary Figure S5.

A) Representative NanoSight analysis of size distribution of exosomes secreted by WM164 and WM983 non-target control and *RAB27A*-KD cells or B16-F10 empty vector control and *Rab27a* CRISPR KO cells. Representative of at least 4 independent experiments.

B) Western blots showing levels of GAPDH, GM130 and Calnexin in exosomes (exo) or cell lysates (CL) from B16-F10 and WM164 control or KD/KO cells as indicated. Proteins were extracted from exosomes secreted by 2×10^7 cells or cell lysates of 2×10^6 cells. Representative of at least 3 independent experiments.

C) Nanosight measurement of number of exosomes and BCA assay of total proteins in the exosomes secreted by WM983C Non-target control or *RAB27A* KD cells. Numbers of exosomes or amount of protein are normalized to

WM983C non-target control cells. Error bars represent the mean ± SEM, n=3. Significance was determined via student t test; ns = not significant.

D) Western blots showing proteins levels of Rab27a in B16-F10 mock transfection control, negative control siRNA#1, negative control siRNA#2 and *Rab27a* siRNA cells. Representative of at least 3 independent experiments.

E) NanoSight measurement of number of exosomes secreted by 10^6 B16-F10 mock control, negative siRNA#1, negative siRNA#2 and *Rab27a* siRNA cells. Exosomes numbers were normalized to B16-F10 negative siRNA#1. Error bars represent the mean ± SEM, n=3 B16-F10 negative siRNA#1 group was compared to other groups via One-way ANOVA and Dunnett's test; ns = not significant.

Supplementary Figure S6.

A) Principal component analysis (PCA) of correlation of three biological repeats within each group (as indicated).

B) Volcano plot of fold change and p-value of expression of proteins of exosomes secreted by WM164 replete cells versus *RAB27A* Sh#1 cells. Differential expressed proteins were determined by more than 1.5-fold change of expression and $P<0.05$ (see highlighted proteins within the red and green boxes).

C) Normalized protein abundance counting of RAB27A, CD63 and TSG101 in the exosomes secreted by WM164 non-target control and *RAB27A* sh#1 cells (indicated as control and Sh#1), error bars represent the mean ± SEM.

D) Normalized protein abundance counting of RAB22A, RAB6B, RAB9A, RAB11A and RAB11B in the exosomes secreted by WM164 non-target

control and sh#1 cells (indicated as control and Sh#1), error bars represent the mean ± SEM.

E) Left: Western blots showing levels of RAB11 and RAB27a in exosomes (Exo) or cell lysates (CL) from WM164 control or sh#1 KD cells as indicated. Western blotting against tubulin was carried out as a loading control. Protein was extracted from exosomes secreted by 2×10^7 cells or cell lysates of 2×10^6 cells. Representative of at least 3 independent experiments.

Right: Western band intensity fold change of RAB11 protein in RAB27A KD exosomes relative to control exosomes. Error bars represent the mean ± SEM of three independent experiments.

F) Normalized protein abundance counting of GPC1 and EPHB4 proteins in the exosomes secreted by WM164 non-target control and Sh#1 cells (indicated as control and Sh#1), error bars represent the mean ± SEM.

G) Western blots showing levels of Glypican-1 (GPC1) in exosomes (Exo) or cell lysates (CL) from WM164 control or sh#1 KD cells as indicated. Western blotting against tubulin was carried out as a loading control. Protein was extracted from exosomes secreted by 2×10^7 cells or cell lysates of 2×10^6 cells. Representative of at least 3 independent experiments.

H) Bar graphs of GO/KEGG terms, each bar represents a term, indicates the number of proteins that changed abundance after RAB27A KD (FDR < 0.05). Color codes the ratio of proteins with higher/lower abundance after RAB27A KD (green: higher abundance in RAB27AKD; red: higher abundance in control). Bar length represents the enrichment score (-log10 FDR).

Figure 1

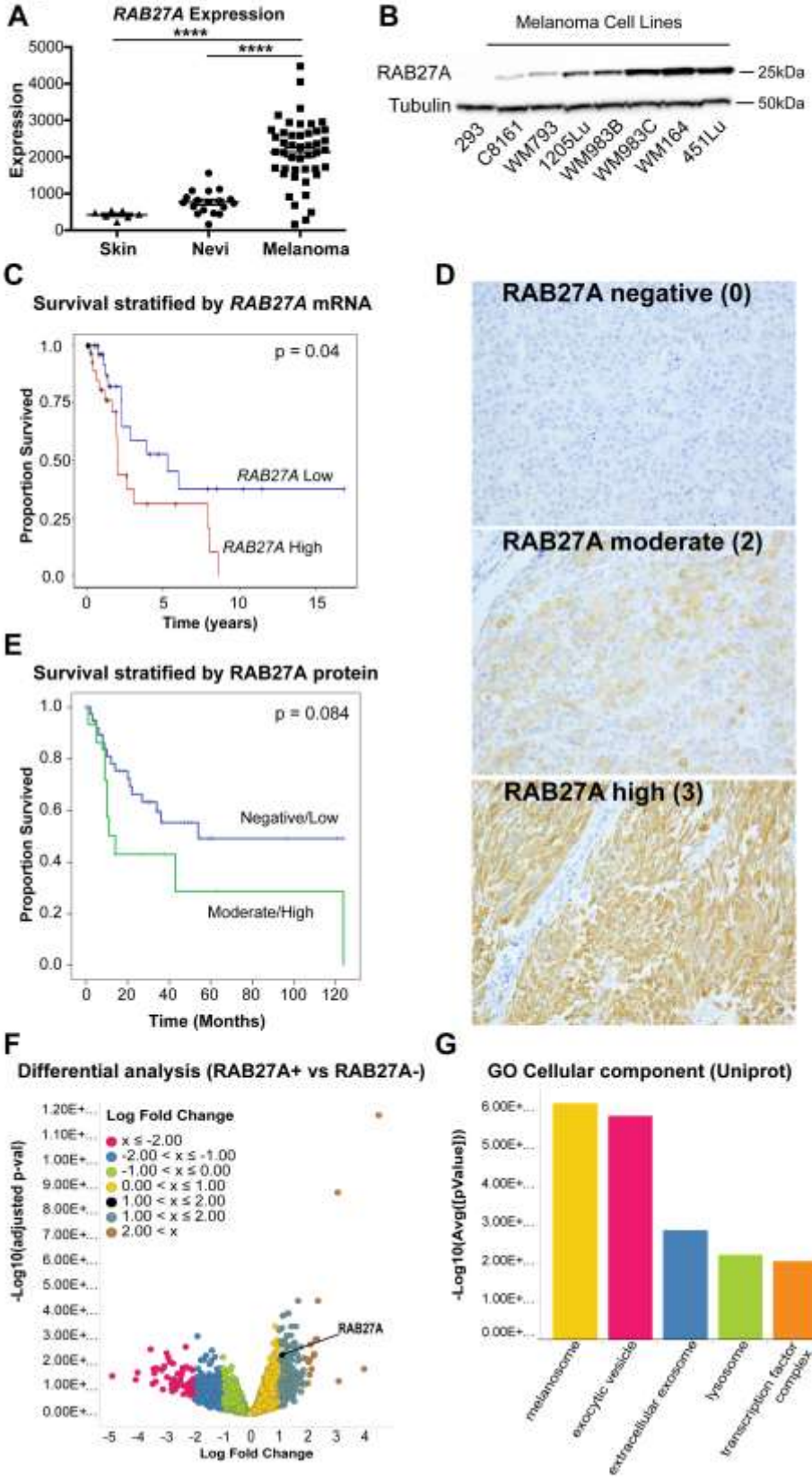

Figure 2

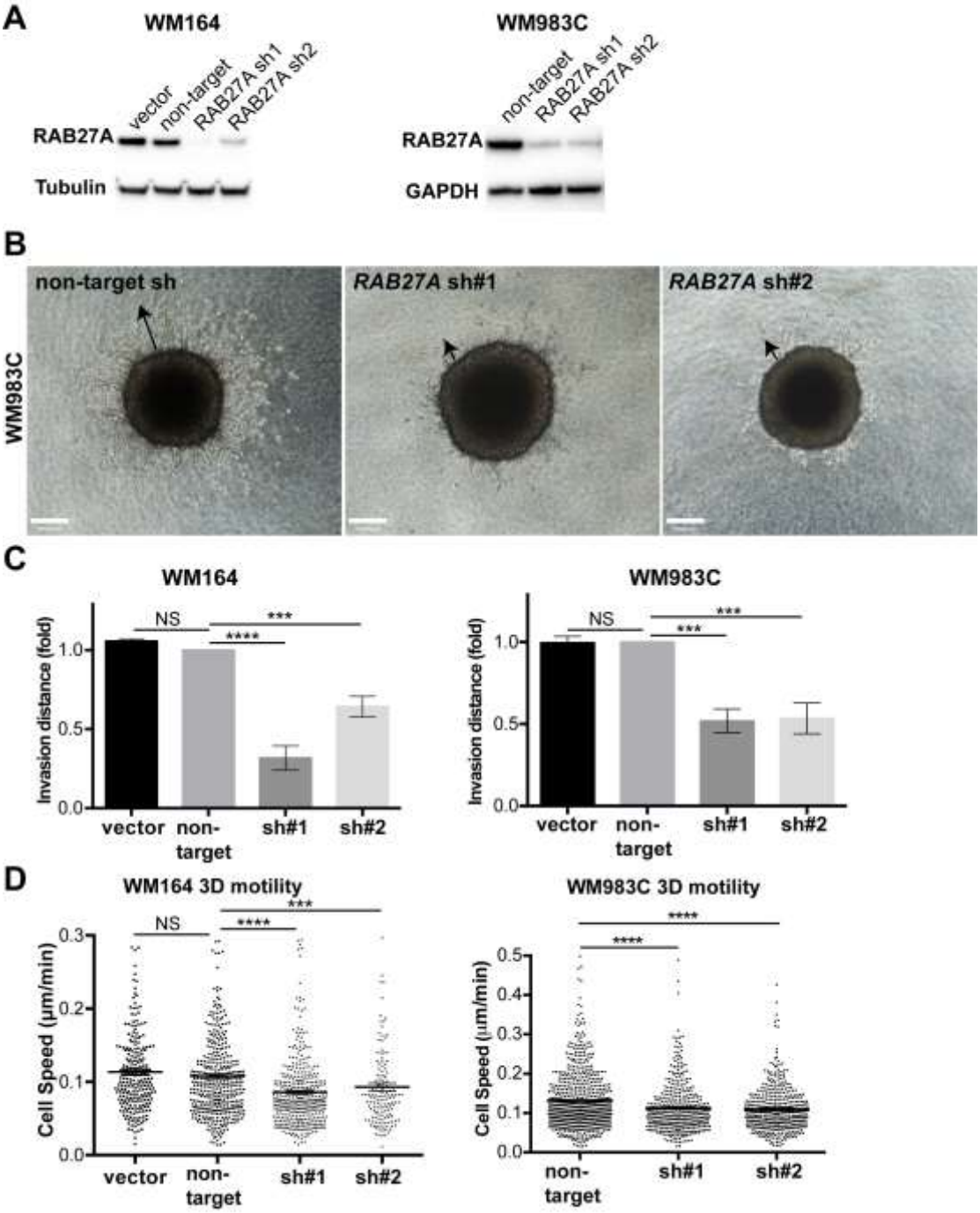

Figure 3

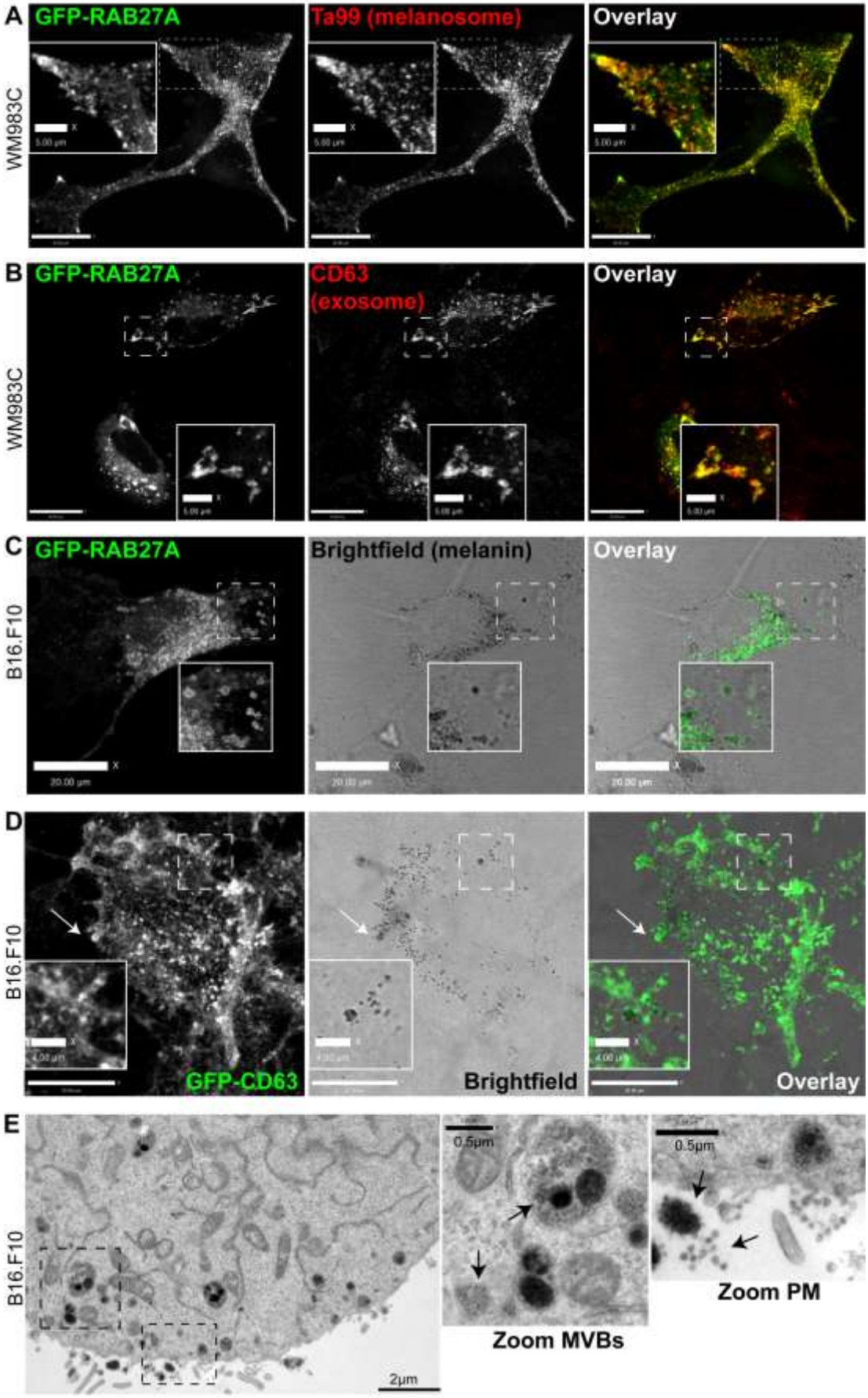

Figure 4

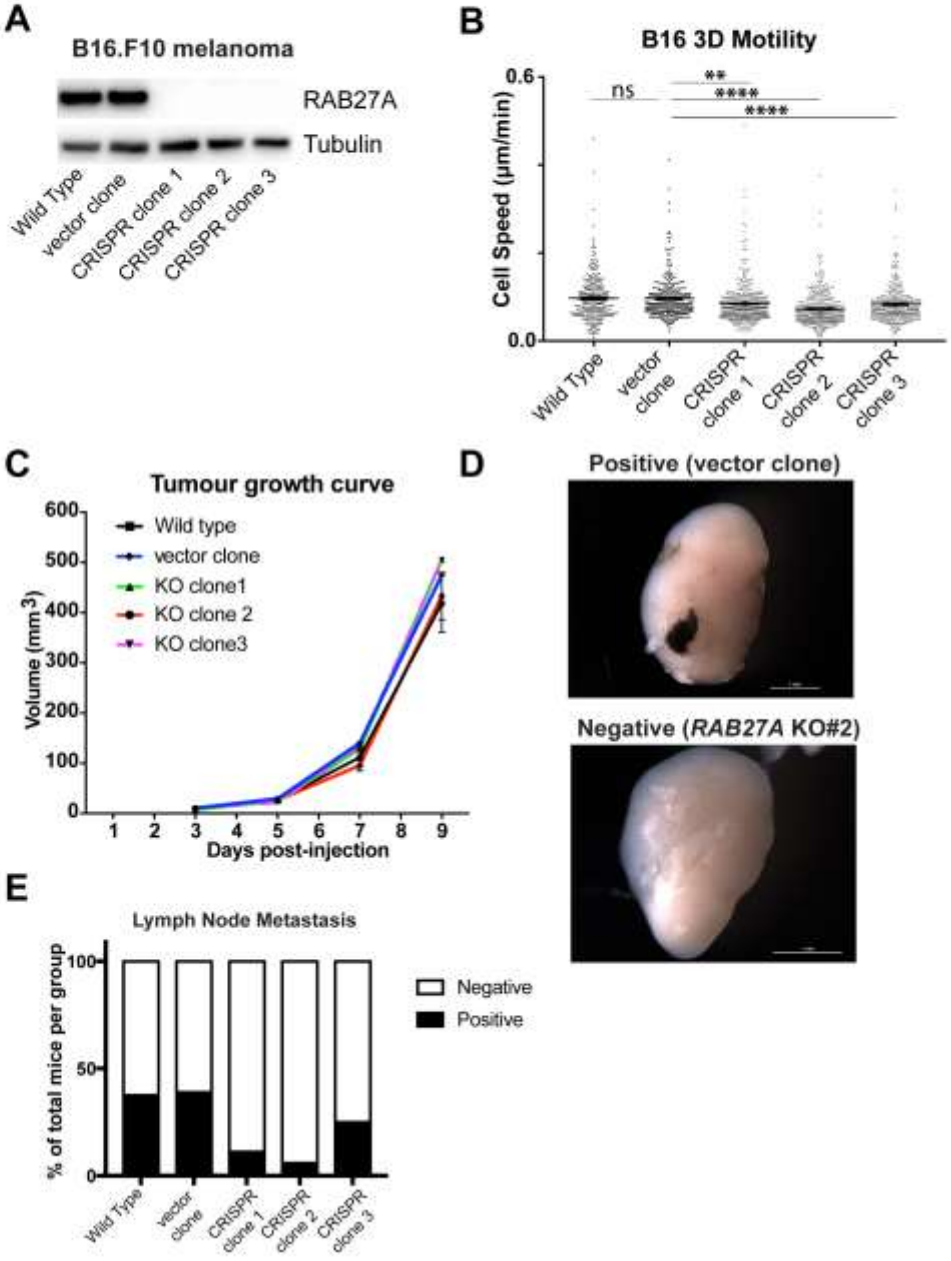

Figure 5

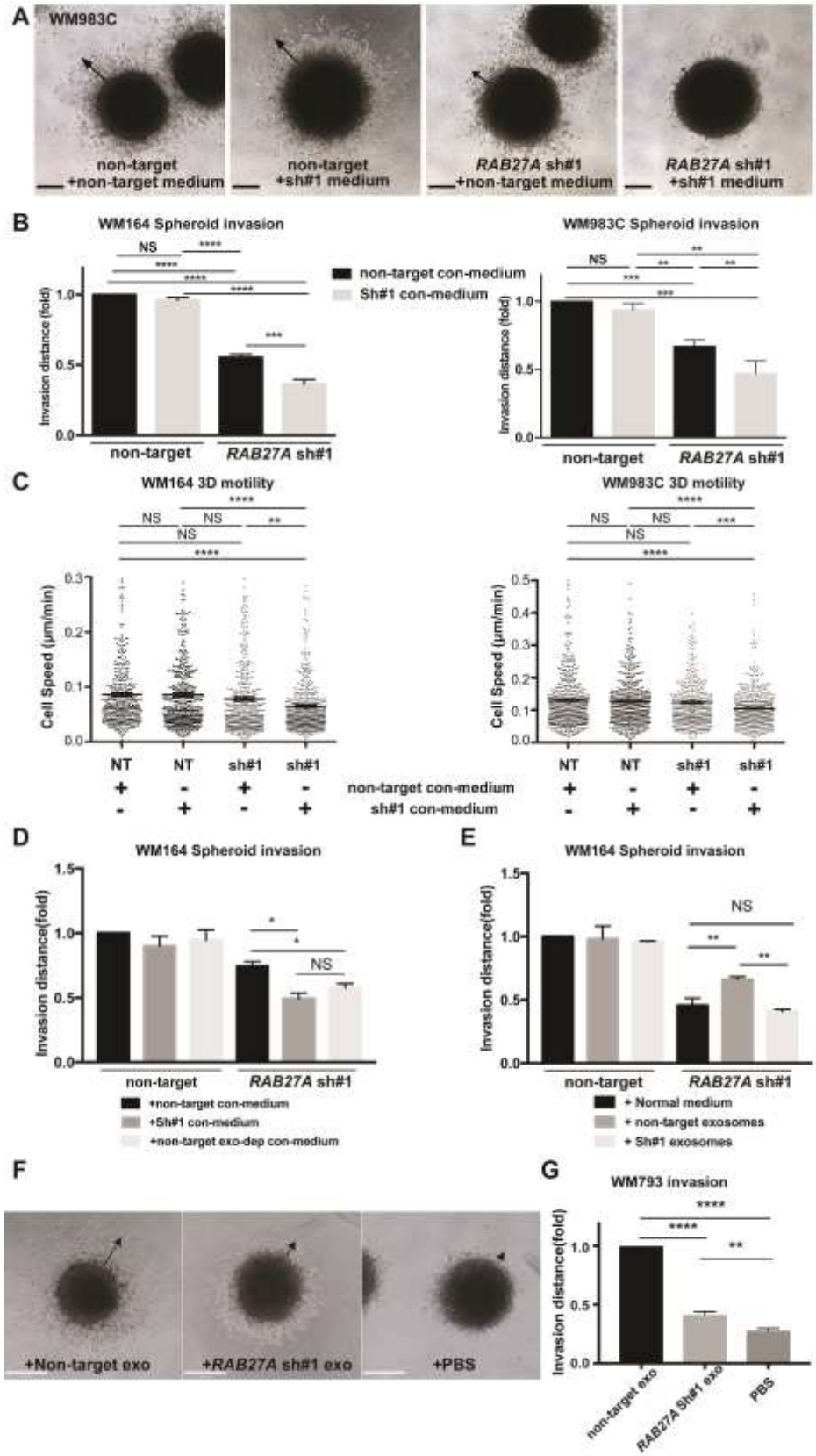

Figure 6

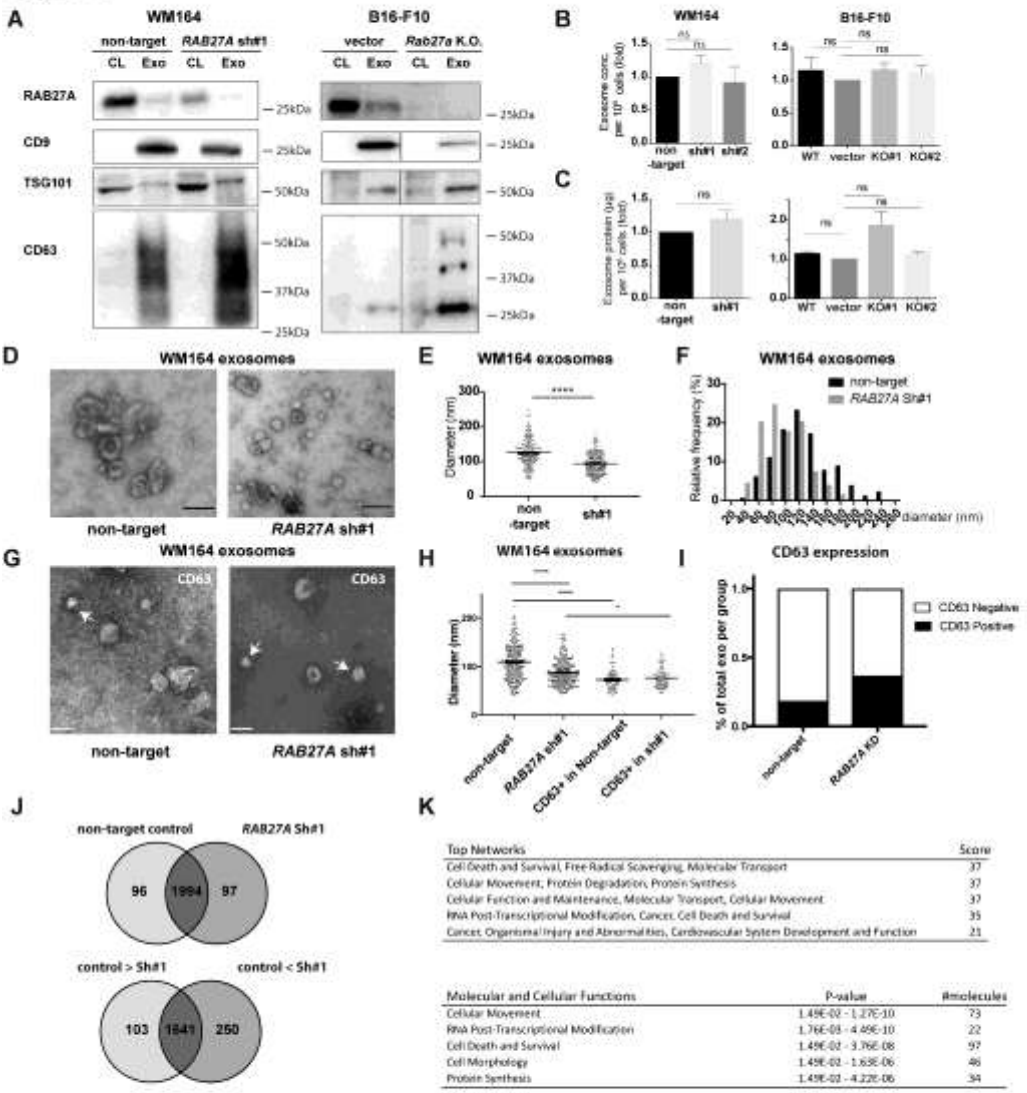

Top Networks	Score
Cell Death and Survival, Free Radical Scavenging, Molecular Transport	37
Cellular Movement, Protein Degradation, Protein Synthesis	37
Cellular Function and Maintenance, Molecular Transport, Cellular Movement	37
RNA Post-Transcriptional Modification, Cancer, Cell Death and Survival	35
Cancer, Organismal Injury and Abnormalities, Cardiovascular System Development and Function	21

Molecular and Cellular Functions	P-value	#molecules
Cellular Movement	1.49E-02 - 1.27E-10	73
RNA Post-Transcriptional Modification	1.76E-08 - 4.49E-10	22
Cell Death and Survival	1.49E-02 - 3.76E-08	97
Cell Morphology	1.49E-02 - 1.63E-06	46
Protein Synthesis	1.49E-02 - 4.22E-06	34